### Title

Network topology and functional connectivity disturbances precede the onset of Huntington's disease




### Journal

Brain, 138(8)

### ISSN

0006-8950



### Authors

Harrington, Deborah L
Rubinov, Mikail
Durgerian, Sally
et al.



### Publication Date

2015-08-01

### DOI

10.1093/brain/awv145

Peer reviewed

doi:10.1093/brain/awv145 BRAIN 2015: 138; 2332–2346 | 2332

BRAIN
A JOURNAL OF NEUROLOGY

# Network topology and functional connectivity disturbances precede the onset of Huntington's disease

**Deborah L. Harrington,[1,2] Mikail Rubinov,[3,4] Sally Durgerian,[5] Lyla Mourany,[6] Christine Reece,[6] Katherine Koenig,[7] Ed Bullmore,[3] Jeffrey D. Long,[8] Jane S. Paulsen[8] for the PREDICT-HD investigators of the Huntington Study Group and Stephen M. Rao[6]**

Cognitive, motor and psychiatric changes in prodromal Huntington's disease have nurtured the emergent need for early interventions. Preventive clinical trials for Huntington's disease, however, are limited by a shortage of suitable measures that could serve as surrogate outcomes. Measures of intrinsic functional connectivity from resting-state functional magnetic resonance imaging are of keen interest. Yet recent studies suggest circumscribed abnormalities in resting-state functional magnetic resonance imaging connectivity in prodromal Huntington's disease, despite the spectrum of behavioural changes preceding a manifest diagnosis. The present study used two complementary analytical approaches to examine whole-brain resting-state functional magnetic resonance imaging connectivity in prodromal Huntington's disease. Network topology was studied using graph theory and simple functional connectivity amongst brain regions was explored using the network-based statistic. Participants consisted of gene-negative controls ($n = 16$) and prodromal Huntington's disease individuals ($n = 48$) with various stages of disease progression to examine the influence of disease burden on intrinsic connectivity. Graph theory analyses showed that global network interconnectivity approximated a random network topology as proximity to diagnosis neared and this was associated with decreased connectivity amongst highly-connected rich-club network hubs, which integrate processing from diverse brain regions. However, functional segregation within the global network (average clustering) was preserved. Functional segregation was also largely maintained at the local level, except for the notable decrease in the diversity of anterior insula intermodular-interconnections (participation coefficient), irrespective of disease burden. In contrast, network-based statistic analyses revealed patterns of weakened frontostriatal connections and strengthened frontal-posterior connections that evolved as disease burden increased. These disturbances were often related to long-range connections involving peripheral nodes and interhemispheric connections. A strong association was found between weaker connectivity and decreased rich-club organization, indicating that whole-brain simple connectivity partially expressed disturbances in the communication of highly-connected hubs. However, network topology and network-based statistic connectivity metrics did not correlate with key markers of executive dysfunction (Stroop Test, Trail Making Test) in prodromal Huntington's disease, which instead were related to whole-brain connectivity disturbances in nodes (right inferior parietal, right thalamus, left anterior cingulate) that exhibited multiple aberrant connections and that mediate executive control. Altogether, our results show for the first time a largely disease burden-dependent functional reorganization of whole-brain networks in prodromal Huntington's disease. Both analytic approaches provided a unique window into brain reorganization that was not related to brain atrophy or motor symptoms. Longitudinal studies currently in progress will chart the course of functional changes to determine the most sensitive markers of disease progression.

1 Department of Radiology, University of California, San Diego, La Jolla, CA, 92093, USA
2 Research Service, VA San Diego Healthcare System, San Diego, CA, 92161, USA
3 Department of Psychiatry, University of Cambridge, Cambridge, CB3 2QQ, UK
4 Churchill College, University of Cambridge, Cambridge, CB3 0DS, UK

Received January 29, 2015. Revised March 6, 2015. Accepted April 4, 2015. Advance Access publication June 9, 2015

5 Department of Neurology, Medical College of Wisconsin, Milwaukee, WI, 53226, USA
6 Schey Centre for Cognitive Neuroimaging, Neurological Institute, Cleveland Clinic, Cleveland, OH, 44195, USA
7 Imaging Sciences, Imaging Institute, Cleveland Clinic, Cleveland, OH, 44195, USA
8 Carver College of Medicine, The University of Iowa, Iowa City, IA, 52242, USA

Correspondence to: Stephen M. Rao, PhD
Schey Centre for Cognitive Neuroimaging
Neurological Institute
Cleveland Clinic
9500 Euclid Avenue / U10
Cleveland, OH 44195, USA
E-mail: raos2@ccf.org

**Keywords:** Huntington disease; resting-state connectivity; network topology; graph theory; network based statistic

**Abbreviations:** AUC = area under the curve; CAP = CAG–age product; NBS = network-based statistic

# Introduction

Huntington disease is a neurodegenerative disorder resulting from a cytosine-adenine-guanine (CAG) repeat expansion in the *HTT* gene. Diagnosis of Huntington's disease is made at the appearance of unequivocal motor signs, yet subtle cognitive (e.g. attention, executive, memory), motor (e.g. chorea, bradykinesia, oculomotor), and psychiatric symptoms (e.g. anxiety, depression, obsessive-compulsiveness) are detected decades earlier during the prodromal phase. With the development of treatments that could delay onset or slow progression of symptoms, there is a need for surrogate markers that are sensitive to changes in neuronal dysfunction during the prodromal phase. Though cognitive variables track disease progression and add to the prediction of time to diagnosis (Harrington *et al.*, 2012; Paulsen *et al.*, 2013, 2014*a*, *b*), striatal volumes are notably robust markers (Aylward *et al.*, 2012; Paulsen *et al.*, 2014*a*, *b*; Ross *et al.*, 2014). However, atrophy of the striatum or cortex (Nopoulos *et al.*, 2010; Harrington *et al.*, 2014) does not characterize the functional topography of disease progression. In this regard, measures of intrinsic functional connectivity from resting-state functional MRI are of keen interest to elucidate the effect of early striatal degeneration on intrinsic activity within the whole brain.

Changes in the spatiotemporal dynamics of synchronization in cognitive and perceptual resting-state networks, identified by independent components analysis, have been of interest owing to the decline in cognition in prodromal Huntington's disease. Initial resting-state functional MRI studies suggest that only some of these networks exhibit functional connectivity disturbances. The dorsal attention network (occipital-parietal) showed decreased synchronization in prodromal Huntington's disease (Poudel *et al.*, 2014*a*), as did the visual network with sensorimotor cortex (Dumas *et al.*, 2013). In contrast, preserved functional connectivity has been observed within the executive (i.e. medial/lateral frontal), working memory (i.e. fronto-parietal), and default mode networks in prodromal Huntington's disease (Dumas *et al.*, 2013; Poudel *et al.*, 2014*a*). Seed-based approaches also found preserved functional connectivity of the isthmus cingulate, a key element of the default mode network (Seibert *et al.*, 2012), in prodromal Huntington's disease.

Thus, initial studies using independent component-derived networks and seed-based approaches indicate that abnormal resting-state functional MRI connectivity may be circumscribed to dorsal attention and visual networks, despite declines in a range of cognitive abilities, including executive functions, attention, visuospatial cognition, and memory (Tabrizi *et al.*, 2009; Duff *et al.*, 2010; Say *et al.*, 2011; Stout *et al.*, 2011; Harrington *et al.*, 2012; Georgiou-Karistianis *et al.*, 2014*a*; Paulsen *et al.*, 2014*a*). Although these analytical approaches have provided valuable insights, they do not provide an understanding of connectivity at the scale of the whole brain, which to date has not been studied in prodromal Huntington's disease. Furthermore, previous resting-state functional MRI studies have not examined functional connectivity as a function of disease burden, as approximated by the time to a manifest diagnosis. Task-related functional MRI, for example, demonstrates that activation patterns depend on the stage of prodromal disease progression (Paulsen *et al.*, 2004; Zimbelman *et al.*, 2007; Wolf *et al.*, 2008; Rao *et al.*, 2014).

The present study used two complementary analytical approaches to examine whole-brain connectivity in prodromal Huntington's disease. The first examined network topology using graph theory, which provides concise summaries of global network interconnectivity, organizational features of groups of nodes, and the extent to which individual regions play an integrative role (Bullmore and Sporns, 2009; Rubinov and Sporns, 2010; van den Heuvel and Sporns, 2013). Owing to the absence of investigations into network topology in Huntington's disease, key properties of functional networks were assessed at global, intermediate, and local scales. The second approach investigated simple functional connectivity amongst every connection linking 300 brain regions using the network-based statistic (NBS) (Zalesky *et al.*, 2010*a*, 2012*a*),

which is a powerful tool for identifying group differences in connectivity strength of clusters of interconnected nodes. Our large sample of prodromal Huntington's disease participants ($n = 48$), with varying stages of disease progression, allowed us to examine the influence of disease burden on network topology and functional connectivity for the first time.

We hypothesized that disturbances in graph theory measures would identify novel properties of abnormal network organization that would be expressed more strongly as disease burden increased. We also hypothesized that a core feature of simple functional connectivity disturbances would be a weakening in frontostriatal connections, possibly owing to prominent structural changes in the basal ganglia (Aylward *et al.*, 2012; Paulsen *et al.*, 2014*b*) and densely interconnected white-matter tracts underlying frontal cortex (Matsui *et al.*, 2014). We also explored relationships between network topology and functional connectivity indices and measures of executive functioning and brain atrophy.

# Materials and methods

## Participants

Data were collected at the Cleveland Clinic and the University of Iowa as part of the larger PREDICT-HD study (Paulsen *et al.*, 2006, 2008, 2014*b*). Ethics committees at both sites approved the study procedures and written informed consent was obtained from participants according to the Declaration of Helsinki. Participants completed genetic testing for the CAG expansion independent from entry into PREDICT-HD; confirmatory DNA testing was conducted after enrolment. A certified examiner completed the Motor Assessment section of the Unified Huntington's Disease Rating Scale (UHDRS; Supplement 1). Examiners rated their confidence level that a participant's motor signs were an indication of Huntington's disease using the five-point Diagnostic Confidence Level (DCL); participants were excluded with a DCL of 4 ($\geq$99% confidence of unequivocal signs of Huntington's disease). The Supplementary material specifies additional exclusion criteria.

The sample consisted of 48 prodromal Huntington's disease participants and 16 gene-negative controls who were offspring of a parent with Huntington's disease, but without the CAG expansion. The prodromal Huntington's participants were stratified into Low, Medium, and High groups (16 subjects per group) based on the CAG-Age Product, computed as CAP = [(age at study entry) $\times$ (CAG repeats $-$ 33.66)], which is a validated index of disease burden in prodromal Huntington's disease (Zhang *et al.*, 2011; Paulsen *et al.*, 2014*b*) (Supplementary material). Cut-offs for the three CAP groups were based on an optimization algorithm from the larger PREDICT-HD cohort ($n > 1000$). Based on this stratification, estimated time to diagnosis is $>$12.78 years, 12.78 to 7.59 years, and $<$7.59 years for the Low, Medium, and High groups, respectively. Table 1 details group characteristics. As expected, the Low group was significantly younger than the High group, but also the Negative group. Though the High group was less educated than the Negative group, mean educational level did not differ among the other prodromal Huntington's groups. There were no group differences in sex or number of subjects scanned at the two sites.

## Cognitive tests

Participants were administered three tests of executive functions that track disease progression in prodromal Huntington's disease (O'Rourke *et al.*, 2011; Paulsen *et al.*, 2013, 2014*a*) including: (i) the Stroop Color and Word Test (color naming, word reading, and interference; total correct in 45 s) (Golden, 1978); (ii) the Symbol Digit Modalities Task (total correct in 90 s) (Smith, 1995); and (iii) the Trail Making Test (Parts A and B; time to complete) (Reitan and Wolfson, 1993).

## Neuroimaging protocol

Both sites used identical Siemens TIM Trio 3 T MRI scanners equipped with a 12-channel receive-only head array. Comparison of phantom data between sites indicated similar image quality and signal-to-noise ratio. Frequent quality assurance scans were performed at each institution to ensure that imaging data were free of scanner artefacts and were comparable across sites. Whole-brain resting-state functional MRI scans were acquired with a gradient-echo, echoplanar pulse sequence [132 repetitions, 31 4.0 mm thick axial slices (no gap); matrix 128 $\times$ 128; in-plane resolution 2 $\times$ 2 mm; echo time/repetition time/flip angle, 29/2800 ms/80°; field of view, 256 $\times$ 256 mm; receiver bandwidth, 1954 Hz/pixel]. Subjects kept their eyes closed during the scan. $T_1$ with $T_1$-weighted inversion recovery turboflash (magnetization-prepared rapid acquisition with gradient echo, MPRAGE) images [GRAPPA factor = 2, 240 coronal slices, thickness = 1 mm, field-of-view = 256 mm $\times$ 256 mm, inversion time/echo time/repetition time/flip angle = 900 ms/3.09 ms/2530 ms/10, matrix = 256 $\times$ 128, receiver bandwidth = 220 Hz/pixel] were acquired for registration with echo planar images and grey matter thickness/volumetric measurements.

## Resting state image analysis

Physiologic noise was estimated using PESTICA (Beall and Lowe, 2007) and was regressed out at the voxel level using RETROICOR (Glover *et al.*, 2000) (Supplementary material). Several procedures were used to meticulously screen resting-state functional MRI scans for motion including visual inspection of resting-state functional MRI time series and correlation maps (Supplementary material). AFNI 3dvolreg (Cox, 1996) was used to retrospectively correct volumetric-level motion. The 3dvolreg program realigns subsequent volumes of time series data to a base volume and outputs volumetric motion parameters for rotation and displacement of each volume to the base volume. Volumetric parameters were then trigonometrically converted to voxel-level displacement and a model of the signal fluctuations was regressed from the time series at each voxel (Bullmore *et al.*, 1999). The groups did not significantly differ in mean and maximum peak-to-peak displacement during the resting-state functional MRI scan ($P > 0.163$) (Supplementary material). Data were spatially

**Table 1 Demographic, clinical and cognitive test variables**

| | Negative | Low | Medium | High | | | |
|---|---|---|---|---|---|---|---|
| | *n* = 16 | *n* = 16 | *n* = 16 | *n* = 16 | *P*[a] | ES[b] | *Post hocs*[c] |
| **Demographic and clinical** | | | | | | | |
| Age (years) | 42.6 (9.2) | 32.6 (9.0) | 39.3 (9.7) | 47.1 (12.6) | 0.0020 | 0.22 | Neg, High > Low |
| Education (years) | 16.0 (1.9) | 14.4 (2.2) | 15.3 (2.5) | 13.9 (2.4) | 0.0470 | 0.12 | Neg > High |
| Sex (% male) | 4 (25) | 1 (6.3) | 5 (31.3) | 2 (12.5) | 0.2510 | – | |
| CAG repeats | – | 41.8 (1.9) | 42.6 (2.6) | 43.6 (3.2) | 0.1380 | 0.08 | |
| CAP score | – | 251.9 (30.2) | 332.3 (18.5) | 439.0 (45.5) | 0.0001 | 0.85 | Low < Med < High |
| UHDRS Motor Score | 5.1 (4.5) | 3.5 (3.8) | 4.9 (4.4) | 13.4 (7.8) | 0.0001 | 0.36 | Neg, Low, Med < High |
| Location scanned (CC, UI) | 4, 12 | 7, 9 | 10, 6 | 7, 9 | 0.2060 | – | |
| **Cognitive** | | | | | | | |
| SDMT | 61.0 (9.8) | 56.4 (10.4) | 56.8 (9.7) | 47.8 (10.6) | 0.0018 | 0.09 | Neg, Medium > High |
| Stroop Color | 88.2 (15.10) | 84.4 (10.6) | 83.1 (10.6) | 68.9 (14.2) | 0.0002 | 0.20 | Neg, Low, Med > High |
| Stroop Word | 110.3 (19.8) | 107.1 (12.4) | 105.8 (16.1) | 84.4 (19.7) | 0.0002 | 0.19 | Neg, Low, Med > High |
| Stroop Interference | 51.4 (9.8) | 51.4 (12.8) | 52.4 (11.2) | 40.2 (10.6) | 0.0064 | 0.12 | Neg, Low, Med > High |
| Trails A | 19.4 (4.4) | 23.7 (7.9) | 21.4 (8.7) | 30.3 (13.1) | 0.0075 | 0.10 | Neg, Med < High |
| Trails B | 51.3 (19.0) | 50.8 (19.0) | 44.3 (8.7) | 83.7 (42.5) | 0.0002 | 0.20 | Neg, Low, Med < High |
| Trails B-A | 31.3 (17.8) | 27.1 (15.8) | 22.8 (9.2) | 53.4 (38.4) | 0.0023 | 0.16 | Neg, Low, Med < High |

[a]*P*-values for age, education, CAG, CAP score, and UHDRS derived from ANOVA; sex and location scanned from chi-square test; all cognitive variables from ANCOVA with age and education as covariates.
[b]ES = effect size; $\eta^2$ for demographic and clinical variables and partial $\eta^2$ for cognitive variables.
[c]Tukey's honestly significant difference; *post hoc* testing on cognitive variables based on means adjusted for age and education.
CC = Cleveland Clinic; UI = University of Iowa; SDMT = Symbol Digit Modality Test (total correct); Stroop = Stroop Color and Word Test (total correct for Color Naming, Word Reading, and Interference subtests); Trails = Trail Making Test, Parts A and B (seconds to complete).

filtered using a Hamming filter, affine transformed to MNI152 stereotactic space, and temporally bandpass-filtered to remove fluctuations $<0.01$ Hz and $>0.1$ Hz. Statistical tests were conducted on the age-standardized residuals of each imaging variable. Scanner site was not significantly associated with any of the imaging variables.

## Cortical and subcortical parcellation

To derive measures of functional connectivity, the cortical surface and subcortical structures were subdivided into nodes. Accurate parcellation is important for accurate mapping of interregional functional connectivity (Zalesky *et al.*, 2010*b*). We used a medium-density resolution of 300 nodes, derived using a spatially constrained clustering method (Craddock *et al.*, 2012) that subdivides regions into similarly sized parcels while optimizing homogeneity of correlations among voxels within each node (Supplementary material). The group parcellation was based on gene-negative participants. However, our main effect tests of group for graph-theory derived measures were largely reproducible when we conducted individual subject parcellations using the current method (Craddock *et al.*, 2012) and another approach that maximizes homogeneity without the constraint of similar parcel sizes (Blumensath *et al.*, 2013) (Supplementary Table 1).

## Network topology analysis

Complex network analyses were conducted on weighted networks using the Brain Connectivity Toolbox (Rubinov and Sporns, 2010). Weights in our matrices represent z-scores of Pearson correlations. Intrinsic time series data are known to have time and spatial correlations that can impact the distribution of correlation values in individual subjects. To normalize the sampling distribution, correlations were converted to z-scores using the method of Lowe *et al.* (1998). Edges were defined by thresholding the connectivity matrix to include z-scores $>0.84$. This threshold was chosen to balance statistical evidence of connectivity with the desire to avoid less reliable sparse networks (Braun *et al.*, 2011; Rubinov and Sporns, 2011; Wang *et al.*, 2011). The threshold excluded negative z-scores, which reduce the reliability of graph theory-based metrics (Wang *et al.*, 2011).

We computed widely-used complex network measures of global, intermediate, and local-scale network organization (Rubinov and Sporns, 2010; van den Heuvel and Sporns, 2011). Global network measures included: 'density', a measure of total connectivity that is equivalent to the average connection weight in the network; 'clustering coefficient', a measure of the propensity of the network to form clusters that is computed as the average fraction of triangles out of all connected triples (Onnela *et al.*, 2005); and 'global efficiency', a measure of the propensity of the network to be globally interconnected that is computed as the average inverse shortest path length between all pairs of nodes (Latora and Marchiori, 2001). Intermediate-scale network measures capture organizational properties of groups of nodes. We focused on the extent to which the network may be said to contain a rich-club or a central core of highly-connected regions (van den Heuvel and Sporns, 2011). We did this by computing the 'rich-club coefficient', defined as the density of connections (average connection weight) between central hub nodes (Colizza *et al.*, 2006). Clustering coefficient, global efficiency, and rich-club coefficient were normalized to the mean value derived from 100 random networks (Rubinov and Sporns, 2010) (Supplementary material), because these measures of network

organization should not be interpreted in isolation. For instance, an increase in global efficiency is not necessarily beneficial if it is accompanied by a reduction in measures such as the clustering coefficient. Indeed, random graphs have very high global efficiency, but very low clustering coefficients, reflecting an imbalance between integration and segregation.

Local measures, which describe the centrality of individual nodes (van den Heuvel and Sporns, 2013; Crossley *et al.*, 2014), included: 'weighted nodal degree', the total sum of weights associated with a node; 'participation coefficient', the diversity of nodal connections between distinct subnetworks or modules (Guimera and Amaral, 2005); and 'eigenvector centrality', a self-referential measure designating the degree to which high eigenvector centrality nodes connect to other high eigenvector centrality nodes. These measures describe the extent to which individual nodes play an integrative role in the network. To compare different node centrality measures, we converted these measures to ranks (van den Heuvel *et al.*, 2010).

## Functional connectivity analysis

Simple functional connectivity disturbances were examined using the NBS, which detects large within-network components that are evaluated statistically using permutation testing (Zalesky *et al.*, 2010*a*, 2012*a*). A test statistic (fitted z-scores) of correlation coefficients was computed for all edges connecting the 300 nodes (i.e. positive and negative correlations). The Negative group and each prodromal Huntington's group were then compared on age-standardized residuals of the fitted z-scores for all edges by applying a threshold of $t \geqslant 3.5$ to form a set of suprathreshold connected clusters (i.e. based on the graph theoretical concept of connected components) at an uncorrected level.

## Structural MRI analyses of brain morphometry

MRI scans were analysed to test for group differences in bilateral regional cortical volume and thickness and subcortical volumes, since hemispheric asymmetries have not been noted across multiple studies (Nopoulos *et al.*, 2010; Aylward *et al.*, 2012; Harrington *et al.*, 2014). Cortical volume and thickness were derived from the Desikan atlas parcellation method (Desikan *et al.*, 2006) in FreeSurfer 5.1 software (Fischl *et al.*, 2004), which demonstrates good test-retest reliability across scanners and sites (Han *et al.*, 2006) (Supplementary material). Volumetric measures were adjusted for total intracranial volume [(volume/intracranial volume) × 100)]. Five subcortical volumes (putamen, globus pallidus, caudate, accumbens, and thalamus) were analysed. ANCOVAs (age-adjusted) tested for group differences in volume and thickness measures, false discovery rate (FDR) corrected for multiple comparisons.

# Results

## Neuropsychological testing

Group differences (ANCOVA; age and education covariates) were found for all cognitive variables (Table 1). The High group performed significantly worse than the Negative group and one or more of the other prodromal Huntington's groups on all tasks.

## Network topology

Tests for group differences on all network topology measures were assessed by permutation testing (100 000) using the Kruskal-Wallis test (group main effect) and *t*-tests (coin in R) for follow-up pairwise group comparisons (Hothorn *et al.*, 2008). Group means for age-adjusted residuals are shown in Fig. 1 (unadjusted group means shown in Supplementary Table 2) for global and intermediate network measures. Significant group effects were found for global efficiency. Planned comparisons demonstrated that global efficiency was increased in the Medium ($P = 0.035$) and High ($P = 0.002$) groups compared to the Negative group and correlated with CAP scores ($r = 0.33$, $P = 0.022$), indicating that efficiency became more like a random network topology as disease burden increased. No significant group differences were observed for density or the average clustering coefficient.

Figure 3 displays the rich-club ratio for each group as a function of node strength (k). A k of 130 was the highest value for which all subjects had data and the k-value functions exhibited no sharp discontinuities. The rich-club coefficient measure was therefore computed by integrating each subject's rich-club coefficients for all node strengths $\leqslant 130$ to compute the area under the curve (AUC). Preliminary analyses demonstrated that the results were not sensitive to the choice of threshold. The main effect of group was significant for rich-club AUC (Fig. 1). Planned comparisons showed that rich-club organization was reduced in the Medium ($P = 0.007$) and the High ($P = 0.001$) groups, with a non-significant trend for a reduction in the Low group ($P = 0.093$). Rich-club AUC negatively correlated with CAP scores ($r = -0.32$, $P = 0.024$), indicating that interconnectivity amongst a central core of highly-connected regions declined with disease burden (Fig. 2).

To characterize the rich-club anatomy, we identified nodes whose strength (k) was $>130$ in 90% of the subjects in one or more of the groups (Supplementary material). Thus, the location of rich-clubs was similar within and across groups. Figure 4 shows the 50 nodes that were identified, placing 17% of the nodes in the rich-club, which is comparable to an anatomical rich-club of 15% of the nodes (van den Heuvel and Sporns, 2011) (Supplementary materials). High-strength nodes were prominent in midline central (right supplementary motor area, bilateral middle cingulate) and posterior (superior parietal, precuneus, cuneus, lingual and fusiform gyrus) cortices, sensorimotor cortex (precentral and postcentral gyrus), lateral temporal (bilateral superior temporal and Heschl's gyrus; right middle temporal) and occipital cortices (superior and middle occipital), and the cerebellum (lobule VI). High node strength of midline anterior and

posterior areas was notable. Critically, group differences in node strength (summed z-score) were not significant for any of the 50 nodes (FDR adjusted). This finding provides converging evidence that the density of connections between rich-club nodes specifically decreased with proximity to diagnosis, rather than node strength.

As for local centrality measures, group differences were non-significant for nodal degree and eigenvector centrality

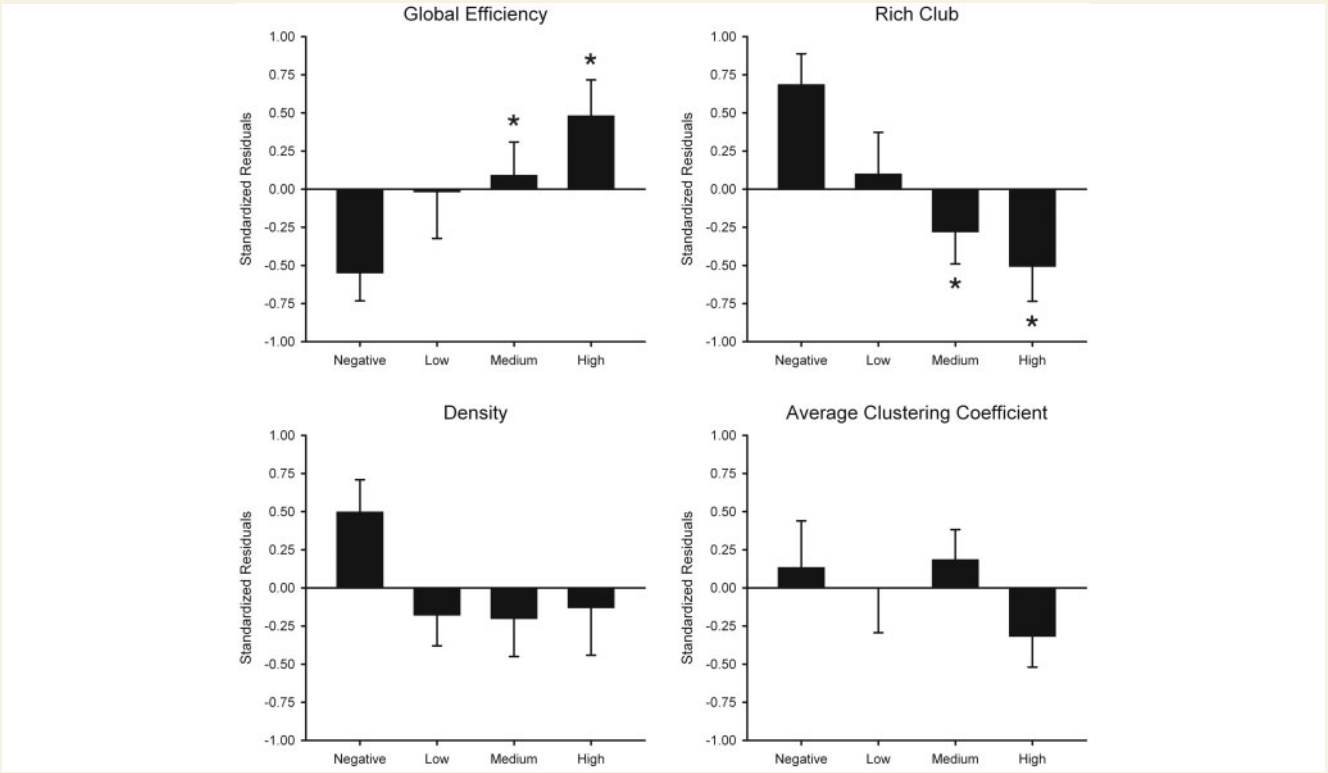


**Figure 1 Network topology measures in the gene-negative and the gene-positive groups.** Bar graphs display the mean (standard error) standardized age-adjusted residuals for global efficiency, rich-club area under the curve (AUC), density, and average clustering coefficient in each group. Plotted values can be negative as they are standardized residuals. Supplementary Table 2 reports the unadjusted means and standard deviations for these measures, for which all values are positive. The main effect of group (Negative, Low, Medium, and High) was significant for global efficiency and rich-club AUC. For these measures, asterisks designate significant differences in the means between the Negative group and a prodromal Huntington's disease group (global efficiency: Medium, $P = 0.035$, High, $P = 0.002$; rich-club AUC: Medium, $P = 0.007$, High, $P = 0.001$).

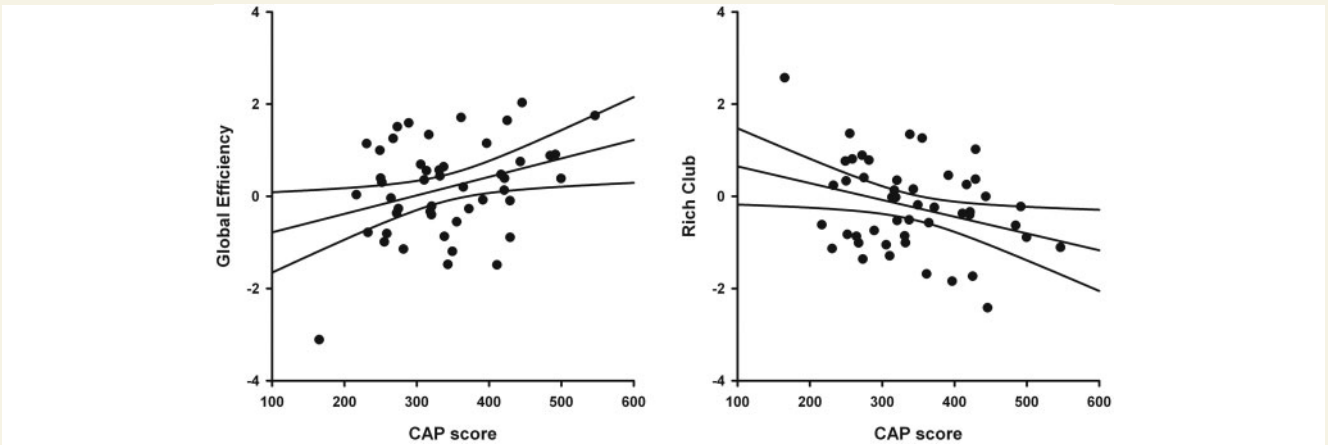


**Figure 2 Association between network topology measures and disease burden in gene-positive participants.** Scatter plots show the relationship between the CAP score and the age-adjusted residuals for global efficiency ($r = 0.33$, $P = 0.022$) and rich-club area under the curve ($r = -0.32$, $P = 0.024$). The solid lines show the best-fitting linear regression line and the 95% confidence intervals.

for all 300 nodes (FDR adjusted). For the participation coefficient, only the left anterior insula showed a significant group effect ($P = 0.00015$; q = 0.045, FDR adjusted). Relative to the Negative group [mean (standard deviation; SD) unadjusted rank = 92.25 (39.14)], the participation coefficient for the anterior insula was ranked lower in the Low [189.88 (85.37), $P = 0.0002$], Medium [143.44 (69.08), $P = 0.01$], and High [197.75 (72.41), $P = 0.00006$] groups and did not correlate with CAP scores.

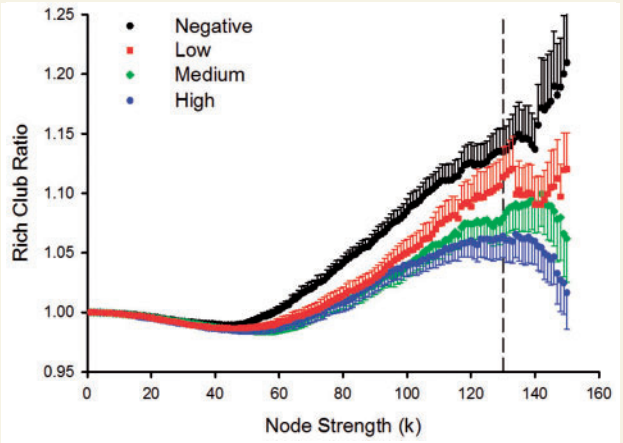


**Figure 3 Rich-club ratio plots for gene-negative and gene-positive groups as a function of node strength.** The graph shows the association between the mean (standard error) ratios of rich-club to a random network as a function of node strength (k) for each of the groups. The figure shows that differences between the Negative and the prodromal Huntington's disease groups emerge as node strength increases. A k-value of 130 was the highest node-strength value for which all subjects had data and the functions were well-behaved, exhibiting no sharp discontinuities (vertical dotted line).

### Association between global efficiency and other network metrics

A stepwise multiple regression analysis, adjusting for CAP scores, tested the association between global efficiency and the other network metrics. Rich-club AUC accounted for a large per cent of the variance ($R^2_{change} = 0.47$; $F_{change} = 50.45$, $P = 1.0 \times 10^{-10}$), followed by the average clustering coefficient ($R^2_{change} = 0.12$; $F_{change} = 18.41$, $P = 0.0001$) and density ($R^2_{change} = 0.04$; $F_{change} = 6.52$, $P = 0.014$). These results indicated that as global efficiency increased, rich-club organization, average clustering, and density decreased.

## Functional connectivity

Permutation testing (5000) was used to identify significant group differences (i.e. negative group versus each prodromal Huntington's group) at the cluster level ($P < 0.05$ corrected). The NBS analyses identified functional connectivity disturbances in prodromal Huntington's disease that were characterized by weaker (Negative > prodromal Huntington's disease) or stronger (prodromal Huntington's disease > Negative) connections relative to

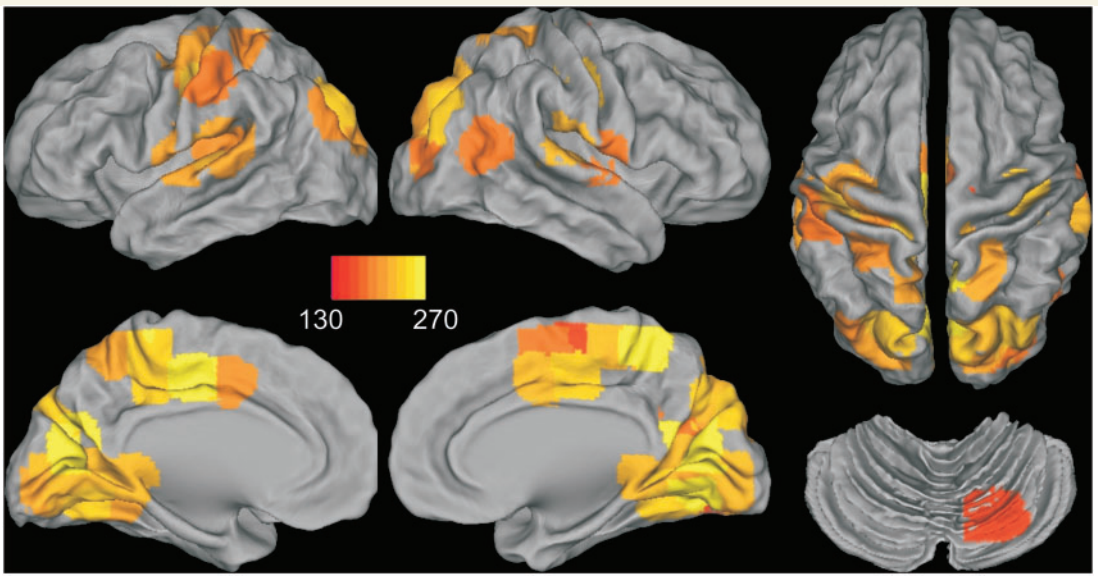


**Figure 4 Rich-club anatomy for the entire sample.** Fifty nodes are shown whose strength (k) was greater than 130 in 90% of the subjects in one or more of the groups. Images are displayed in neurological view (left side = left hemisphere). The red–yellow colour bar denotes the average node strength across all subjects. High-strength nodes were prominent in midline central [right supplementary motor area (SMA), bilateral middle cingulate] and posterior (superior parietal, precuneus, cuneus, lingual and fusiform gyrus) cortices, sensorimotor cortex (precentral and postcentral gyrus), lateral temporal (bilateral superior temporal and Heschl's gyrus; right middle temporal) and occipital (superior and middle occipital) cortices, and the cerebellum (lobule VI). The node strength of midline anterior and posterior areas was particularly notable. Group differences in node strength were not significant (FDR adjusted) for any of these nodes.

the Negative group (Fig. 5). Functional connectivity was preserved in the Low group. The number of weakened connections within frontal cognitive-control centres (e.g. anterior and middle cingulate, medial superior frontal, superior frontal gyrus, middle frontal gyrus, inferior frontal gyrus), the anterior insula, and the hippocampus/parahippocampus was greatest in the High group, but was also found in the Medium group (Supplementary Table 3). Many aberrant edges involved interhemispheric connections. The High group also showed weakened basal ganglia connections (i.e. caudate with anterior cingulate and thalamus; putamen with middle frontal gyrus), whereas the Medium group exhibited weakened connections within ventral attention centres (lingual gyrus, calcarine cortex, superior/middle temporal and occipital), which also showed reduced connectivity to frontal areas.

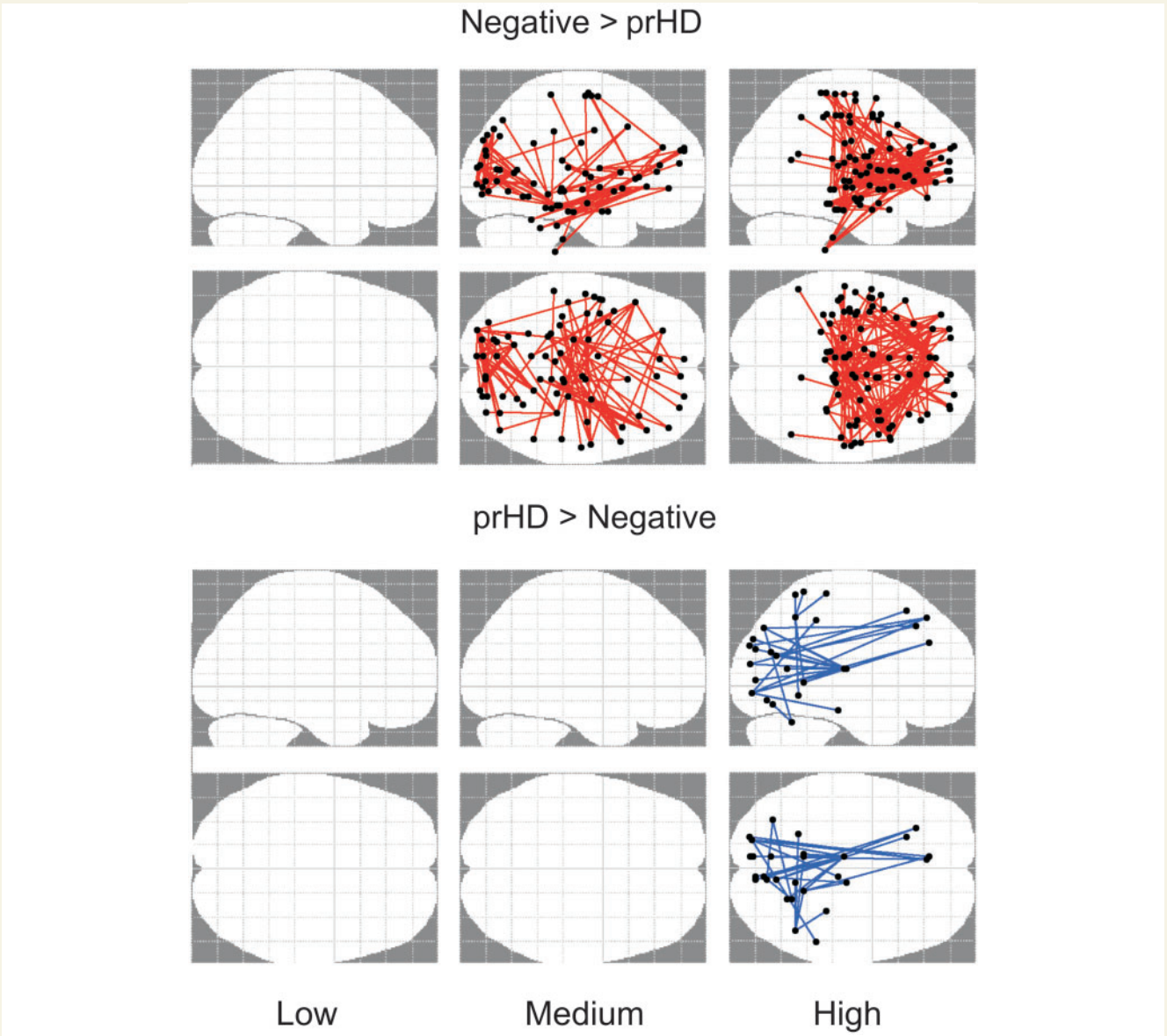


**Figure 5 Aberrant functional connectivity in the gene-positive groups.** To identify anatomical sources of functional connectivity disturbances in prodromal Huntington's disease (prHD), the fitted z-scores of correlation coefficients (standardized age-adjusted residuals) for all edges connecting the 300 nodes were compared between the Negative group and each of the prodromal Huntington's disease groups using the network-based statistic. The glass brains illustrate the aberrant functional connections that were identified for each prodromal Huntington's disease group. The brains at the top (Negative > prHD) display functional connections that were weaker (red edges) in each prodromal Huntington's disease group relative to the Negative group. The brains at the bottom (prHD > Negative) display functional connections that were stronger (blue edges) in each prodromal Huntington's disease group relative to the Negative group. Empty glass brains signify no group differences in functional connectivity.

Only the High group showed stronger connectivity than the Negative group (Fig. 5). Here, connections of ventral attention areas (e.g. lingual gyrus, calcarine cortex, fusiform gyrus, superior/middle temporal and occipital) and parietal cortex (precuneus, inferior parietal lobe) were stronger with frontal cortex (medial superior frontal gyrus, superior frontal gyrus, middle frontal gyrus, sensorimotor), thalamus, and cerebellum (Supplementary Table 3).

### Association between aberrant connectivity and network topology

The sum of the z-score residuals were computed separately for all aberrant connections that were weaker and stronger in the NBS analysis (Fig. 5) in one or more of the prodromal Huntington's groups. A stepwise multiple regression analysis, adjusting for CAP scores, tested the association between the sum of aberrant weakened and strengthened connectivity and the network topology metrics. For weakened connections, rich-club AUC accounted for a large per cent of the variance ($R^2_{change} = 0.34$; $F_{change} = 26.6$, $P < 0.0001$), followed by density ($R^2_{change} = 0.10$; $F_{change} = 8.72$, $P = 0.005$), indicating that as the connectivity of aberrantly weakened connections decreased, so did rich-club organization and density. For strengthened connections, decreased rich-club organization ($R^2_{change} = 0.07$; $F_{change} = 4.81$, $P = 0.03$) and increased density ($R^2_{change} = 0.07$; $F_{change} = 5.28$, $P = 0.026$) were weakly associated with an increase in the connectivity of aberrantly strengthened connections. The correlation between rich-club AUC and aberrant connectivity may be associated with their partial overlap in anatomy (e.g. sensorimotor, precentral and postcentral gyrus, cingulate and fusiform gyrus, precuneus, superior temporal and occipital areas). However, only 5% of the weakened and strengthened connections were between two rich-club hubs (rich-club connection), whereas only one node of an edge was a rich-club hub for 35% of the aberrant connections (hub connection) (van den Heuvel and Sporns, 2011). Thus, the majority of aberrant connections (60%) involved two peripheral nodes.

### Whole-brain functional connectivity of aberrant nodes

Some nodes exhibited abnormal connectivity with multiple regions in the Medium and/or High groups. As disturbances in these nodes might be an important source of abnormal communication, we explored the effects of disease burden on 'whole-brain connectivity' within this subset of nodes. To identify these nodes, the frequency by which each of the 300 nodes appeared in an aberrant connection in the Medium and/or High group was plotted. The point at which the distribution of the number of aberrant edges began to asymptote defined the nodes with the most aberrant connections (range = 8 to 25 aberrant connections; Supplementary Table 4). The sum of z-scores for each of these nodes and their edges was calculated to obtain a measure of a node's 'whole-brain' functional connectivity.

Group differences in the sum of z-scores for each node was then tested by permutation testing (100 000) using the Kruskal-Wallis test (group main effect) and *t*-tests for follow-up pairwise group comparisons (Fig. 6). Left anterior cingulate connectivity was weakened in the Low and High groups, whereas left middle occipital gyrus connectivity was weakened in only the Medium group. All prodromal Huntington's groups showed weakened left hippocampus, right thalamus, bilateral insula, left inferior frontal gyrus, and right Heschl's gyrus connectivity relative to the Negative group. CAP scores did not correlate with the summed z-scores for any of these regions. Strengthened whole-brain connectivity of the right inferior parietal lobe also differed in prodromal Huntington's disease, positively correlating with CAP scores ($r = 0.31$, $P = 0.032$).

## Correlations of cognitive variables with network and functional connectivity

In prodromal Huntington's disease participants, stepwise multiple regression analyses tested associations between abnormal network topology and functional connectivity measures and cognitive variables (Symbol Digit Modalities Test, Stroop Color, Stroop Interference, and Trails B-A). The analyses correlated age-adjusted residuals for the imaging measures with age- and education-adjusted residuals for the cognitive measures. No significant associations were found between cognitive measures and global efficiency, rich-club AUC, or the participation coefficient for the left anterior insula (FDR adjusted). Likewise, no significant associations were found between cognitive measures and connectivity of aberrantly weakened and strengthened connections (FDR adjusted). Motor symptoms (UHDRS) also did not correlate with any of these measures.

For the abnormal 'node-based whole-brain functional connectivity measures', four stepwise regression models were tested in which frontal (left anterior cingulate, bilateral inferior frontal gyrus), right parietal, and thalamic nodes were used as predictor variables for each of the four cognitive measures, since these regions are particularly associated with executive control. Figure 7 shows that poorer Stroop Color Naming performance (lower values) correlated with stronger right inferior parietal lobe functional connectivity [$F(1,46) = 10.41$, $P = 0.002$ uncorrected, $P < 0.05$ FDR corrected; $r = -0.434$], whereas poorer Stroop Interference performance correlated with stronger right thalamus connectivity [$F(1,46) = 14.87$, $P = 0.0004$ uncorrected, $P < 0.05$ FDR corrected; $r = -0.494$]. Poorer Trails B-A performance (higher values) correlated with weaker connectivity of the left anterior cingulate [$F(1,46) = 5.70$, $P = 0.02$ uncorrected, $P < 0.05$ FDR corrected; $r = -0.332$]. No other connectivity measures added to the prediction of performances on these variables. Although some of these relationships (e.g. correlation of

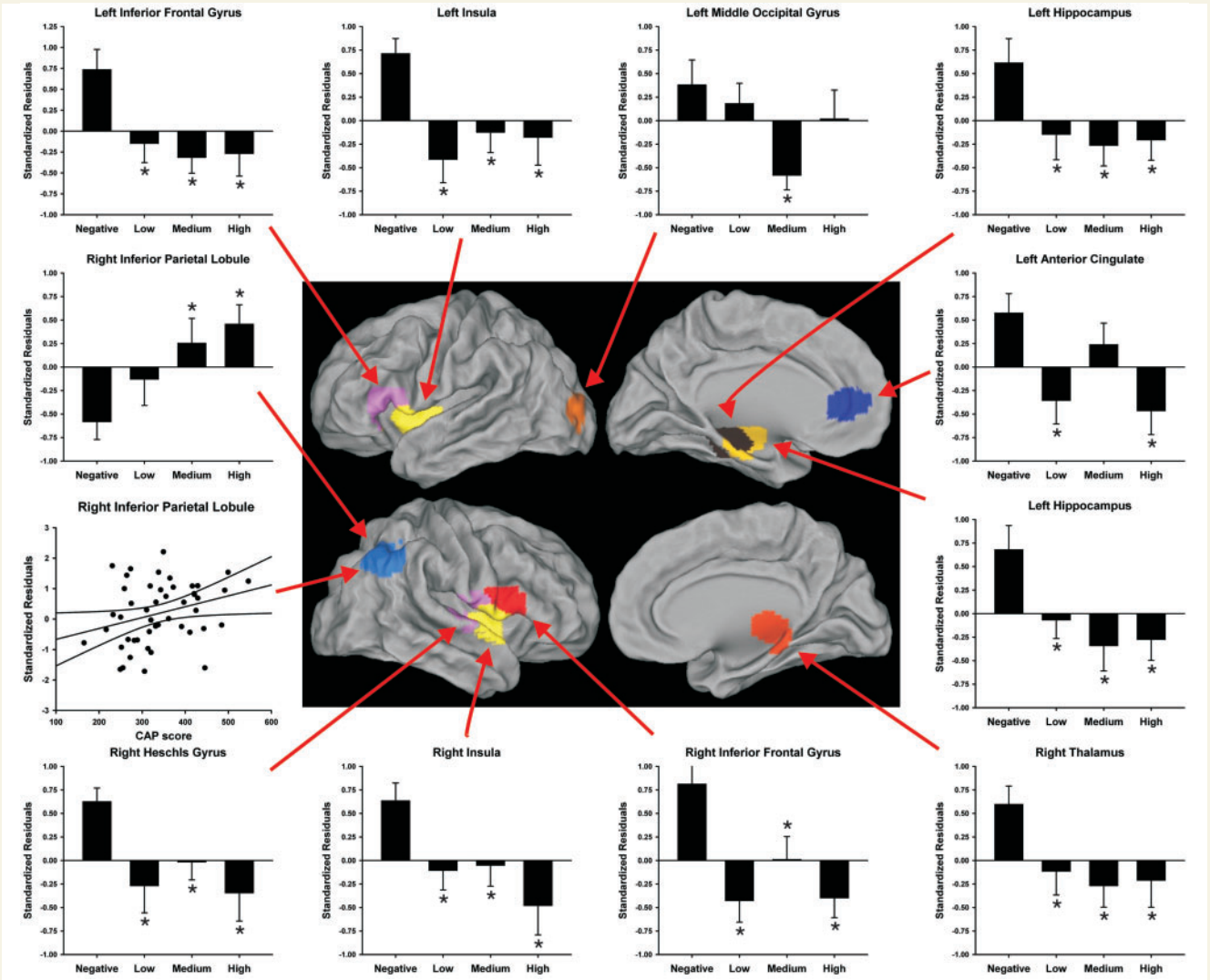


**Figure 6 Whole-brain functional connectivity of nodes with the highest number of weakened and strengthened aberrant connections in gene-positive individuals.** Displayed nodes are those showing a significant main effect of group (Negative, Low, Medium, High) (Supplementary Table 4). Their anatomical location is shown on lateral and medial sections of brains. The bar graphs display the mean (standard error) of the whole-brain summed z-scores (standardized age-adjusted residuals) for each group. An asterisk designates significant differences in the means between the Negative group and a prodromal Huntington's disease group. The scatter plot (*left*) illustrates the significant association between CAP scores and whole-brain functional connectivity of the right inferior parietal lobe ($r = 0.31$, $P = 0.032$).

Trails B-A with anterior cingulate connectivity) were partly driven by the High group's poorer performance (Fig. 7), none of them were confounded by motor symptoms.

## Network and functional connectivity correlations with brain morphometry

Group differences in cortical thickness and volume were not significant after FDR correction (Supplementary Tables 5 and 6). As expected, group differences in volumes of bilateral putamen, globus pallidus, caudate, and nucleus accumbens were found (Supplementary Table 7), largely due to atrophy in the High group compared to the Negative and/or Low groups. Subcortical volumes did not correlate with abnormal network topology or functional connectivity measures (FDR adjusted).

# Discussion

Our results revealed, for the first time, abnormalities in whole-brain intrinsic functional connectivity in prodromal Huntington's disease that increased with disease burden. Graph theory analyses showed that global network inter-connectivity approximated a random network topology as proximity to diagnosis neared and was associated with decreased connectivity within the rich-club network core. However, average clustered connectivity between a node and its nearest neighbours was preserved. The centrality of

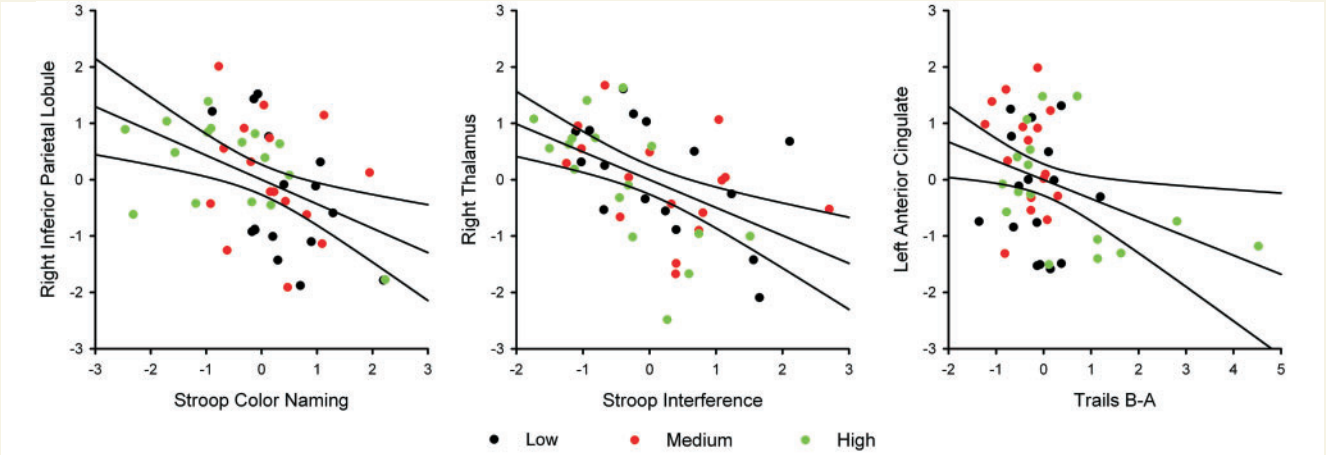


**Figure 7 Association between whole-brain functional connectivity in regions of interest and cognitive performances in gene-positive participants.** Graphs plot the age- and education-adjusted residuals for the cognitive measures against the age-adjusted residuals of the regional summed z-scores in the prodromal Huntington's disease subjects. The solid lines on scatter plots show the best-fitting linear regression line and the 95% confidence intervals. Black, red, and green dots designate participants in the Low, Medium, and High CAP groups, respectively. *Left*: Association between Stroop Color Naming and whole-brain functional connectivity of the right inferior parietal lobule ($r = -0.434$, $P = 0.002$). *Middle*: Association between Stroop Interference and whole-brain connectivity of the right thalamus ($r = -0.494$, $P = 0.0004$). *Right*: Association between Trails B-A and whole-brain connectivity of the left anterior cingulate ($r = -0.332$, $P = 0.02$).

individual regions in promoting communication was also stable, except for the left anterior insula, which occupied a less central role in intermodular integration, irrespective of disease burden. In contrast, NBS analyses revealed patterns of weakened frontostriatal and strengthened frontal-posterior functional connections that evolved as disease burden increased. These connectivity disturbances were often associated with long-range connections involving peripheral nodes or interhemispheric connections. Notably, we found a robust association between weaker connectivity and decreased rich-club organization, indicating that whole-brain simple connectivity partially expressed disturbances in the communication amongst highly connected hubs, which form a backbone that integrates processing from diverse brain regions (van den Heuvel *et al.*, 2012; Vertes *et al.*, 2014). However, network topology metrics and NBS connectivity components did not correlate with cognitive functioning. Rather, cognitive variables correlated with whole-brain functional connectivity of specific nodes (right inferior parietal, right thalamus, left anterior cingulate) that exhibited multiple aberrant connections and that mediate executive control, in support of their relevancy to cognitive decline during the prodromal phase. Aberrant network topology and functional connectivity were not related to brain atrophy or motor symptoms, demonstrating that whole-brain connectivity measures provide a unique window into the reorganization of the brain in the prodromal phase.

## Network topology disturbances

The changes observed in network topology appear related to altered network organization rather than connectivity, as the average global weight of connections was preserved in prodromal Huntington's disease. This contrasts with other diseases wherein altered network topology is often confounded by a loss in the average strength of connections (Liu *et al.*, 2008; Lynall *et al.*, 2010; Rudie *et al.*, 2013). Increased global efficiency as a function of disease burden may suggest that the number of topological shortcuts between brain regions progressively increases with proximity to a diagnosis (Bullmore and Sporns, 2009), thereby resulting in higher global integration. This effect was strongly associated with a loss in rich-club organization. Thus, Huntington's disease seems to target a central core of highly-connected regions thought to promote efficient information integration between disparate brain regions and when damaged cause disintegration of the system as a whole (van den Heuvel and Sporns, 2011; Collin *et al.*, 2014; Crossley *et al.*, 2014; Vertes *et al.*, 2014). Indeed, we found a non-significant trend for reduced rich-club organization in the Low group, possibly signifying deterioration in rich-club organization decades before diagnosis. The anatomy of the rich-club was prominent in known highly-connected hubs including sensorimotor, superior/middle temporal, and auditory cortices (Achard *et al.*, 2006; Tomasi and Volkow, 2011; Grayson *et al.*, 2014) and midline central and posterior areas (Hagmann *et al.*, 2008; Tomasi and Volkow, 2010, 2011; Crossley *et al.*, 2013; van den Heuvel and Sporns, 2013), which contain key elements of the default mode network. Yet studies in prodromal Huntington's disease that used seed-based and independent component-based methods found preserved functioning of the default mode network or key elements (Seibert *et al.*, 2012; Dumas *et al.*, 2013; Poudel *et al.*, 2014*a*). At the same time, the progressive loss in rich-club organization of sensorimotor and visual areas is compatible

with previous findings of reduced connectivity in these structures in prodromal Huntington's disease (Dumas *et al.*, 2013; Poudel *et al.*, 2014*a*). However, the present results suggest more extensive aberrant connectivity likely due to our whole-brain approaches, which characterized different properties of regional connectivity than previously studied. Our results indicate that changes during the prodromal period may be better distinguished by the communication between central hubs *per se*, owing to the high cost that their damage confers on global efficiency (van den Heuvel and Sporns, 2011). This conclusion was bolstered by the absence of group differences in node strength for any of the rich-club regions. We note that rich-club analysis in functional networks may overestimate the extent to which hubs are densely connected, due to the transitive nature of correlation coefficients (Zalesky *et al.*, 2012*b*). However, because such transitivity is present to the same extent in all subjects, it is unlikely to alter our main results.

Importantly, functional segregation (average clustering) within the global network remained stable, compatible with preserved resting-state functional MRI in visual, auditory, and cerebellar networks in prodromal Huntington's disease (Poudel *et al.*, 2014*a*), yet differed from diseases in which cognition is markedly altered and clustering at the global level is reduced (Lynall *et al.*, 2010; Liu *et al.*, 2014). Stable functional segregation was also maintained regionally, except for the left anterior insula, which occupied a less central role in intermodular integration (participation coefficient), even in the Low group, suggesting that it may be an early marker of brain dysfunction. The anterior insula is a functional hub (Zuo *et al.*, 2012; van den Heuvel and Sporns, 2013; Collin *et al.*, 2014; Grayson *et al.*, 2014) that is highly interconnected with cortical association regions and the striatum (Chikama *et al.*, 1997) and that supports focal attention and integrative functions (Nelson *et al.*, 2010; Kelly *et al.*, 2012). Thus, reduced intermodular integration may explain the abnormal anterior insula activation in prodromal Huntington's disease during various cognitive tasks (Zimbelman *et al.*, 2007; Gray *et al.*, 2013; Georgiou-Karistianis *et al.*, 2014*b*; Rao *et al.*, 2014).

## Functional connectivity disturbances

The NBS analyses demonstrated weakened and strengthened connectivity that was expressed most strongly in the High group. Weakened connections corresponded well to the frontostriatal network, but also included the thalamus, anterior insula, and memory centres. Notably, weakened edges were frequently long-range interhemispheric connections, possibly linked to white-matter changes in the corpus callosum and frontal cortex (Rosas *et al.*, 2010; Matsui *et al.*, 2014) and striatal pathway deterioration (Aylward *et al.*, 2012; Poudel *et al.*, 2014*b*). Altered frontostriatal intrinsic connectivity has not been previously found in prodromal Huntington's disease, despite the importance of these networks in executive functioning. Similar network disturbances surfaced in the Medium group, although striatal connectivity was not weakened, possibly because atrophy was restricted to the putamen in our sample. Network reorganization in the Medium group was also characterized by weakened connectivity within ventral attention centres, where connectivity with frontal areas was also diminished. In contrast, long-distance connectivity of ventral attention and parietal areas with frontal and subcortical areas (thalamus, cerebellum) was stronger only in the High group, possibly signifying compensatory intermodular integration between systems, which coactivate during attention-demanding tasks. Interestingly, reconfiguration of networks during cognitive performance is particularly marked by changes in long-range connections (Crossley *et al.*, 2013; Hermundstad *et al.*, 2013), which promote integration and may partly underlie cognitive decline in prodromal Huntington's disease.

For nodes containing multiple aberrant connections, whole-brain connectivity was usually weakened irrespective of disease burden, except for the right inferior parietal lobe, wherein whole-brain connectivity strength increased with disease burden. Although not identified as rich-club hubs by our analyses, these nodes are important centres for cognitive control (anterior cingulate, inferior frontal gyrus), integration and attention (anterior insula, right thalamus, right inferior parietal lobe), and memory (hippocampus), consistent with the diversity of cognitive changes in the prodromal phase (Harrington *et al.*, 2012; Paulsen *et al.*, 2013, 2014*a*, *b*). Intriguingly, most of these nodes were components of the rich-club in a meta-analysis of task-related functional MRI (Crossley *et al.*, 2013), consistent with the reconfiguration of high-degree hubs during cognition (Hermundstad *et al.*, 2013). Thus, abnormal intrinsic connectivity of peripheral nodes may also disrupt information integration and serve as early markers of network changes.

## Cognitive correlations with network topology and functional connectivity

Emerging research indicates that various properties of network efficiency correlate with intelligence and attention in healthy adults (van den Heuvel *et al.*, 2009; Giessing *et al.*, 2013). Yet in our study, cognitive measures were not associated with aberrant network topology metrics or the connectivity of aberrantly weakened and strengthened connections (NBS). Although surprising, changes in the brain can occur years before behavioural manifestations of a disease are observable clinically. Indeed, cognitive changes in prodromal Huntington's disease are subtle (Harrington *et al.*, 2012) and often not clinically significant (Duff *et al.*, 2010). At the same time, summary measures of network organization or connectivity may not be sensitive to subtle changes in specific executive functions, which are governed by specialized brain networks. Indeed, we found

that changes in executive functions known to track disease progression longitudinally in prodromal Huntington's disease (Paulsen *et al.*, 2014*a*), correlated with the connectivity of selected regions. Worse performance on measures of selective attention, including Stroop Color Naming and interference correlated with stronger whole-brain connectivity of the right inferior parietal lobe and the right thalamus, respectively. These findings may reflect compensation in the inferior parietal lobe and thalamus, which mediate top-down attentional control (Hopfinger *et al.*, 2000; Corbetta *et al.*, 2008) and coordinate communication amongst attentional and arousal networks (Portas *et al.*, 1998; Shipp, 2004). These results are particularly noteworthy because the Stroop test is one of the most robust measures of longitudinal cognitive change in prodromal Huntington's disease (Paulsen *et al.*, 2014*a*) and is a strong predictor of time to manifest diagnosis (Paulsen *et al.*, 2014*b*). In contrast, poorer cognitive flexibility (Trails B-A) was associated with weaker connectivity of the anterior cingulate. This finding comports with research demonstrating that the anterior cingulate plays a central role in switching and maintenance of task set (Dosenbach *et al.*, 2007; Leber *et al.*, 2008; Economides *et al.*, 2014). Altogether, these neurocognitive associations elucidate potential mechanisms of cognitive decline on key cognitive markers of disease progression (Paulsen *et al.*, 2014*a*), independent of motor symptoms.

# Conclusion

This is the first study to demonstrate abnormal and preserved network topology properties during the prodromal phase of Huntington's disease. These results contrasted with functional connectivity analyses, which revealed regional patterns of weakened and strengthened connectivity, especially in long-range connections between peripheral nodes and interhemispheric connections. Summary measures from both approaches (global efficiency, NBS weakened connections) were strongly associated with rich-club organization, suggesting that both metrics partially expressed disturbances in the functioning of hubs that are thought to be central for efficient integration of information (van den Heuvel *et al.*, 2012; Crossley *et al.*, 2014). Both approaches also demonstrated that functional reorganization of whole-brain networks advanced as proximity to diagnosis neared, yet regional connectivity disturbances in nodes containing multiple aberrant connections were typically noted decades before an expected diagnosis. Our findings contrast with previous reports of connectivity disturbances in prodromal Huntington's disease that were more circumscribed (Dumas *et al.*, 2013; Poudel *et al.*, 2014*a*). While this discrepancy likely relates in part to our whole-brain analytic approaches, which measure different dimensions of connectivity, both approaches revealed aberrant connectivity of a different sort in sensorimotor, parietal and occipital areas. In addition, when disease burden is ignored as in past studies, this can mask functional changes that emerge as individuals approach a diagnosis.

We also found that connectivity disturbances in selected nodes were associated with key markers of executive functioning in the prodromal phase, whereas summary measures of network topology and functional connectivity were not. Studies are needed that assess functioning in a range of cognitive and behavioural domains (Paulsen *et al.*, 2014*b*) to better evaluate the sensitivity of summary and regional connectivity metrics to changes in clinical variables. Longitudinal studies currently in progress will chart the course of changes in network topology and whole-brain functional connectivity to determine the most sensitive functional markers of disease progression.

# Acknowledgements

We thank the University of Iowa and Cleveland Clinic PREDICT-HD sites, the study participants, the National Research Roster for Huntington Disease Patients and Families, the Huntington's Disease Society of America, and the Huntington Study Group. We acknowledge the assistance of Hans J. Johnson, Vincent A. Magnotta, Mark J. Lowe, and Jeremy H. Bockholt. These results were presented in poster format at the 4th Biennial Conference on Resting State Brain Connectivity, Cambridge, MA, 11-13 September 2014. The content is solely the responsibility of the authors and does not necessarily represent the official views of the National Institutes of Health.

# Funding

This work was supported by grants from the National Institutes of Health, National Institute of Neurological Disorders and Stroke (5RO1NS040068, 1U01NS082083, 5R01NS054893) and the CHDI Foundation (A-5008). D.L.H. was supported by a grant from the Department of Veterans Affairs (CX000146). M.R. was supported by a National Alliance for Research on Schizophrenia and Depression Young Investigator grant (19490) and an Isaac Newton Trust grant for research purposes (13.07(q)).

# Supplementary material

Supplementary material is available at *Brain* online.

# References

Achard S, Salvador R, Whitcher B, Suckling J, Bullmore E. A resilient, low-frequency, small-world human brain functional network with highly connected association cortical hubs. J Neurosci 2006; 26: 63–72.

Aylward EH, Liu D, Nopoulos PC, Ross CA, Pierson RK, Mills JA, et al. Striatal volume contributes to the prediction of onset of Huntington disease in incident cases. Biol Psychiatry 2012; 71: 822–8.

Beall EB, Lowe MJ. Isolating physiologic noise sources with independently determined spatial measures. Neuroimage 2007; 37: 1286–300.

Blumensath T, Jbabdi S, Glasser MF, Van Essen DC, Ugurbil K, Behrens TE, et al. Spatially constrained hierarchical parcellation of the brain with resting-state fMRI. Neuroimage 2013; 76: 313–24.

Braun U, Plichta MM, Esslinger C, Sauer C, Haddad L, Grimm O, et al. Test-retest reliability of resting-state connectivity network characteristics using fMRI and graph theoretical measures. Neuroimage 2011; 59: 1404–12.

Bullmore E, Sporns O. Complex brain networks: graph theoretical analysis of structural and functional systems. Nat Rev Neurosci 2009; 10: 186–98.

Bullmore ET, Brammer MJ, Rabe-Hesketh S, Curtis VA, Morris RG, Williams SC, et al. Methods for diagnosis and treatment of stimulus-correlated motion in generic brain activation studies using fMRI. Hum Brain Mapp 1999; 7: 38–48.

Chikama M, McFarland NR, Amaral DG, Haber SN. Insular cortical projections to functional regions of the striatum correlate with cortical cytoarchitectonic organization in the primate. J Neurosci 1997; 17: 9686–705.

Colizza V, Flammini A, Serrano MA, Vespignani A. Detecting rich--club ordering in complex networks. Nat. Phys 2006; 2: 110–15.

Collin G, Sporns O, Mandl RC, van den Heuvel MP. Structural and functional aspects relating to cost and benefit of rich club organization in the human cerebral cortex. Cereb Cortex 2014; 24: 2258–67.

Corbetta M, Patel G, Shulman GL. The reorienting system of the human brain: from environment to theory of mind. Neuron 2008; 58: 306–24.

Cox RW. AFNI: software for analysis and visualization of functional magnetic resonance neuroimages. Comp Biomed Res 1996; 29: 162–73.

Craddock RC, James GA, Holtzheimer PE, III, Hu XP, Mayberg HS. A whole brain fMRI atlas generated via spatially constrained spectral clustering. Hum Brain Mapp 2012; 33: 1914–28.

Crossley NA, Mechelli A, Scott J, Carletti F, Fox PT, McGuire P, et al. The hubs of the human connectome are generally implicated in the anatomy of brain disorders. Brain 2014; 137: 2382–95.

Crossley NA, Mechelli A, Vertes PE, Winton-Brown TT, Patel AX, Ginestet CE, et al. Cognitive relevance of the community structure of the human brain functional coactivation network. Proc Natl Acad Sci USA 2013; 110: 11583–88.

Desikan RS, Segonne F, Fischl B, Quinn BT, Dickerson BC, Blacker D, et al. An automated labeling system for subdividing the human cerebral cortex on MRI scans into gyral based regions of interest. Neuroimage 2006; 31: 968–80.

Dosenbach NU, Fair DA, Miezin FM, Cohen AL, Wenger KK, Dosenbach RA, et al. Distinct brain networks for adaptive and stable task control in humans. Proc Natl Acad Sci USA 2007; 104: 11073–78.

Duff K, Paulsen J, Mills J, Beglinger LJ, Moser DJ, Smith MM, et al. Mild cognitive impairment in prediagnosed Huntington disease. Neurology 2010; 75: 500–7.

Dumas EM, van den Bogaard SJ, Hart EP, Soeter RP, van Buchem MA, van der Grond J, et al. Reduced functional brain connectivity prior to and after disease onset in Huntington's disease. Neuroimage Clin 2013; 2: 377–84.

Economides M, Guitart-Masip M, Kurth-Nelson Z, Dolan RJ. Anterior cingulate cortex instigates adaptive switches in choice by integrating immediate and delayed components of value in ventromedial prefrontal cortex. J Neurosci 2014; 34: 3340–49.

Fischl B, van der Kouwe A, Destrieux C, Halgren E, Segonne F, Salat DH, et al. Automatically parcellating the human cerebral cortex. Cereb Cortex 2004; 14: 11–22.

Georgiou-Karistianis N, Long JD, Lourens SG, Stout JC, Mills JA, Paulsen JS. Movement sequencing in Huntington disease. World J Biol Psychiatry 2014a; 15: 459–71.

Georgiou-Karistianis N, Stout JC, Dominguez DJ, Carron SP, Ando A, Churchyard A, et al. Functional magnetic resonance imaging of working memory in Huntington's disease: cross-sectional data from the IMAGE-HD study. Hum Brain Mapp 2014b; 35: 1847–64.

Giessing C, Thiel CM, Alexander-Bloch AF, Patel AX, Bullmore ET. Human brain functional network changes associated with enhanced and impaired attentional task performance. J Neurosci 2013; 33: 5903–14.

Glover GH, Li TQ, Ress D. Image-based method for retrospective correction of physiological motion effects in fMRI: RETROICOR. Magn Reson Med 2000; 44: 162–7.

Golden CJ. Stroop color and word test: a manual for clinical and experimental uses. Chicago: Skoelting; 1978.

Gray MA, Egan GF, Ando A, Churchyard A, Chua P, Stout JC, et al. Prefrontal activity in Huntington's disease reflects cognitive and neuropsychiatric disturbances: the IMAGE-HD study. Exp Neurol 2013; 239: 218–28.

Grayson DS, Ray S, Carpenter S, Iyer S, Dias TG, Stevens C, et al. Structural and functional rich club organization of the brain in children and adults. PLoS One 2014; 9: e88297.

Guimera R, Amaral LA. Cartography of complex networks: modules and universal roles. J Stat Mech 2005; 2005: nihpa35573.

Hagmann P, Cammoun L, Gigandet X, Meuli R, Honey CJ, Wedeen VJ, et al. Mapping the structural core of human cerebral cortex. PLoS Biol 2008; 6: e159.

Han X, Jovicich J, Salat D, van der Kouwe A, Quinn B, Czanner S, et al. Reliability of MRI-derived measurements of human cerebral cortical thickness: the effects of field strength, scanner upgrade and manufacturer. Neuroimage 2006; 32: 180–94.

Harrington DL, Liu D, Smith MM, Mills JA, Long JD, Aylward EH, et al. Neuroanatomical correlates of cognitive functioning in prodromal Huntington disease. Brain Behav 2014; 4: 29–40.

Harrington DL, Smith MM, Zhang Y, Carlozzi NE, Paulsen JS. Cognitive domains that predict time to diagnosis in prodromal Huntington disease. J Neurol Neurosurg Psychiatry 2012; 83: 612–19.

Hermundstad AM, Bassett DS, Brown KS, Aminoff EM, Clewett D, Freeman S, et al. Structural foundations of resting-state and task-based functional connectivity in the human brain. Proc Natl Acad Sci USA 2013; 110: 6169–74.

Hopfinger JB, Buonocore MH, Mangun GR. The neural mechanisms of top-down attentional control. Nat Neurosci 2000; 3: 284–91.

Hothorn T, Hornik K, van de Wiel MA, Zeileis A. Implementing a class of permutation tests: the coin Package. J Stat Softw 2008; 28: 1–23.

Kelly C, Toro R, Di MA, Cox CL, Bellec P, Castellanos FX, et al. A convergent functional architecture of the insula emerges across imaging modalities. Neuroimage 2012; 61: 1129–42.

Latora V, Marchiori M. Efficient behavior of small-world networks. Phys Rev Lett 2001; 87: 198701.

Leber AB, Turk-Browne NB, Chun MM. Neural predictors of moment-to-moment fluctuations in cognitive flexibility. Proc Natl Acad Sci USA 2008; 105: 13592–97.

Liu Y, Liang M, Zhou Y, He Y, Hao Y, Song M, et al. Disrupted small-world networks in schizophrenia. Brain 2008; 131: 945–961.

Liu Y, Yu C, Zhang X, Liu J, Duan Y, Alexander-Bloch AF, et al. Impaired long distance functional connectivity and weighted network architecture in Alzheimer's disease. Cereb Cortex 2014; 24: 1422–35.

Lowe MJ, Mock BJ, Sorenson JA. Functional connectivity in single and multislice echoplanar imaging using resting-state fluctuations. Neuroimage 1998; 7: 119–32.

Lynall ME, Bassett DS, Kerwin R, McKenna PJ, Kitzbichler M, Muller U, et al. Functional connectivity and brain networks in schizophrenia. J Neurosci 2010; 30: 9477–87.

Matsui JT, Vaidya JG, Johnson HJ, Magnotta VA, Long JD, Mills JA, et al. Diffusion weighted imaging of prefrontal cortex in prodromal Huntington's disease. Hum Brain Mapp 2014; 35: 1562–73.
Nelson SM, Dosenbach NU, Cohen AL, Wheeler ME, Schlaggar BL, Petersen SE. Role of the anterior insula in task-level control and focal attention. Brain Struct Funct 2010; 214: 669–80.
Nopoulos PC, Aylward EH, Ross CA, Johnson HJ, Magnotta VA, Juhl AR, et al. Cerebral cortex structure in prodromal Huntington disease. Neurobiol Dis 2010; 40: 544-554.
O'Rourke JJ, Beglinger LJ, Smith MM, Mills J, Moser DJ, Rowe KC, et al. The trail making test in prodromal Huntington disease: contributions of disease progression to test performance. J Clin Exp Neuropsychol 2011; 33: 567–79.
Onnela JP, Saramaki J, Kertesz J, Kaski K. Intensity and coherence of motifs in weighted complex networks. Phys Rev E Stat Nonlin Soft Matter Phys 2005; 71: 065103.
Paulsen JS, Hayden M, Stout JC, Langbehn DR, Aylward E, Ross CA, et al. Preparing for preventive clinical trials: the Predict-HD study. Arch Neurol 2006; 63: 883–90.
Paulsen JS, Langbehn DR, Stout JC, Aylward E, Ross CA, Nance M, et al. Detection of Huntington's disease decades before diagnosis: the Predict-HD study. J Neurol Neurosurg Psychiatry 2008; 79: 874–80.
Paulsen JS, Long JD, Johnson HJ, Aylward EH, Ross CA, Williams JK, et al. Clinical and biomarker changes in premanifest Huntington disease show trial feasibility: a decade of the PREDICT-HD study. Front Aging Neurosci 2014a; 6: 78.
Paulsen JS, Long JD, Ross CA, Harrington DL, Erwin CJ, Williams JK, et al. Prediction of manifest Huntington's disease with clinical and imaging measures: a prospective observational study. Lancet Neurol 2014b; 13: 1193–201.
Paulsen JS, Smith MM, Long JD. Cognitive decline in prodromal Huntington disease: implications for clinical trials. J Neurol Neurosurg Psychiatry 2013; 84: 1233–9.
Paulsen JS, Zimbelman JL, Hinton SC, Langbehn DR, Leveroni CL, Benjamin ML, et al. fMRI biomarker of early neuronal dysfunction in presymptomatic Huntington's disease. AJNR Am J Neuroradiol 2004; 25: 1715–21.
Portas CM, Rees G, Howseman AM, Josephs O, Turner R, Frith CD. A specific role for the thalamus in mediating the interaction of attention and arousal in humans. J Neurosci 1998; 18: 8979–89.
Poudel GR, Egan GF, Churchyard A, Chua P, Stout JC, Georgiou-Karistianis N. Abnormal synchrony of resting state networks in premanifest and symptomatic Huntington disease: the IMAGE-HD study. J Psychiatry Neurosci 2014a; 39: 87–96.
Poudel GR, Stout JC, Dominguez DJ, Salmon L, Churchyard A, Chua P, et al. White matter connectivity reflects clinical and cognitive status in Huntington's disease. Neurobiol Dis 2014b; 65: 180–7.
Rao JA, Harrington DL, Durgerian S, Reece C, Mourany L, Koenig K, et al. Disrupton of response inhibition circuits in prodromal Huntington disease. Cortex 2014; 58: 72–85.
Reitan RM, Wolfson D. The halstead-reitan neuropsychological test battery: theory and clinical interpretation. Tucson: Neuropsychology Press; 1993.
Rosas HD, Lee SY, Bender AC, Zaleta AK, Vangel M, Yu P, et al. Altered white matter microstructure in the corpus callosum in Huntington's disease: implications for cortical "disconnection". Neuroimage 2010; 49: 2995–3004.
Ross CA, Aylward EH, Wild EJ, Langbehn DR, Long JD, Warner JH, et al. Huntington disease: natural history, biomarkers and prospects for therapeutics. Nat Rev Neurol 2014; 10: 204–16.
Rubinov M, Sporns O. Complex network measures of brain connectivity: uses and interpretations. Neuroimage 2010; 52: 1059–69.
Rubinov M, Sporns O. Weight-conserving characterization of complex functional brain networks. Neuroimage 2011; 56: 2068–79.
Rudie JD, Brown JA, Beck-Pancer D, Hernandez LM, Dennis EL, Thompson PM, et al. Altered functional and structural brain network organization in autism. Neuroimage Clin 2013; 2: 79–94.
Say MJ, Jones R, Scahill RI, Dumas EM, Coleman A, Santos RC, et al. Visuomotor integration deficits precede clinical onset in Huntington's disease. Neuropsychologia 2011; 49: 264–70.
Seibert TM, Majid DS, Aron AR, Corey-Bloom J, Brewer JB. Stability of resting fMRI interregional correlations analyzed in subject-native space: a one-year longitudinal study in healthy adults and premanifest Huntington's disease. Neuroimage 2012; 59: 2452–63.
Shipp S. The brain circuitry of attention. Trends Cogn Sci 2004; 8: 223–30.
Smith A. symbol digit modalities test: manual. Los Angeles, CA: Western Psychological Services; 1995.
Stout JC, Paulsen JS, Queller S, Solomon AC, Whitlock KB, Campbell JC, et al. Neurocognitive signs in prodromal Huntington disease. Neuropsychol 2011; 25: 1–14.
Tabrizi SJ, Langbehn DR, Leavitt BR, Roos RA, Durr A, Craufurd D, et al. Biological and clinical manifestations of Huntington's disease in the longitudinal TRACK-HD study: cross-sectional analysis of baseline data. Lancet Neurol 2009; 8: 791–801.
Tomasi D, Volkow ND. Functional connectivity density mapping. Proc Natl Acad Sci USA 2010; 107: 9885–90.
Tomasi D, Volkow ND. Functional connectivity hubs in the human brain. Neuroimage 2011; 57: 908–17.
van den Heuvel MP, Kahn RS, Goni J, Sporns O. High-cost, high-capacity backbone for global brain communication. Proc Natl Acad Sci USA 2012; 109: 11372–77.
van den Heuvel MP, Mandl RC, Stam CJ, Kahn RS, Hulshoff Pol HE. Aberrant frontal and temporal complex network structure in schizophrenia: a graph theoretical analysis. J Neurosci 2010; 30: 15915–26.
van den Heuvel MP, Sporns O. Rich-club organization of the human connectome. J Neurosci 2011; 31: 15775–86.
van den Heuvel MP, Sporns O. Network hubs in the human brain. Trends Cogn Sci 2013; 17: 683–96.
van den Heuvel MP, Stam CJ, Kahn RS, Hulshoff Pol HE. Efficiency of functional brain networks and intellectual performance. J Neurosci 2009; 29: 7619–24.
Vertes PE, Alexander-Bloch A, Bullmore ET. Generative models of rich clubs in Hebbian neuronal networks and large-scale human brain networks. Philos Trans R Soc Lond B Biol Sci 2014; 369.
Wang JH, Zuo XN, Gohel S, Milham MP, Biswal BB, He Y. Graph theoretical analysis of functional brain networks: test-retest evaluation on short- and long-term resting-state functional MRI data. PLoS One 2011; 6: e21976.
Wolf RC, Sambataro F, Vasic N, Schonfeldt-Lecuona C, Ecker D, Landwehrmeyer B. Altered frontostriatal coupling in pre-manifest Huntington's disease: effects of increasing cognitive load. Eur J Neurol 2008; 15: 1180–90.
Zalesky A, Cocchi L, Fornito A, Murray MM, Bullmore E. Connectivity differences in brain networks. Neuroimage 2012a; 60: 1055–62.
Zalesky A, Fornito A, Bullmore E. On the use of correlation as a measure of network connectivity. Neuroimage 2012b; 60: 2096–106.
Zalesky A, Fornito A, Bullmore ET. Network-based statistic: identifying differences in brain networks. Neuroimage 2010a; 53: 1197–207.
Zalesky A, Fornito A, Harding IH, Cocchi L, Yucel M, Pantelis C, et al. Whole-brain anatomical networks: does the choice of nodes matter? Neuroimage 2010b; 50: 970–83.
Zhang Y, Long JD, Mills JA, Warner JH, Lu W, Paulsen JS. Indexing disease progression at study entry with individuals at-risk for Huntington disease. Am J Med Genet B Neuropsychiatry Genet 2011; 156B: 751–63.
Zimbelman JL, Paulsen JS, Mikos A, Reynolds NC, Hoffmann RG, Rao SM. fMRI detection of early neural dysfunction in preclinical Huntington's disease. J Int Neuropsychol Soc 2007; 13: 758–69.
Zuo XN, Ehmke R, Mennes M, Imperati D, Castellanos FX, Sporns O, et al. Network centrality in the human functional connectome. Cereb Cortex 2012; 22: 1862–75.